

# Square-root Floquet topological phases and time crystals

Raditya Weda Bomantara\*

*Centre for Engineered Quantum Systems, School of Physics,  
University of Sydney, Sydney, New South Wales 2006, Australia*

(Dated: November 30, 2021)

Periodically driven (Floquet) phases are attractive due to their ability to host unique physical phenomena with no static counterparts. We propose a general approach in nontrivially devising a square-root version of existing Floquet phases, applicable both in noninteracting and interacting setting. The resulting systems are found to yield richer physics that is otherwise absent in the original counterparts and is robust against parameter imperfection. These include the emergence of Floquet topological superconductors with arbitrarily many zero,  $\pi$ , and  $\pi/2$  edge modes, as well as  $4T$ -period Floquet time crystals in disordered and disorder-free systems ( $T$  being the driving period). Remarkably, our approach can be repeated indefinitely to obtain a  $2^n$ -th-root version of a given system, thus allowing for the discovery and systematic construction of a family of exotic Floquet phases.

## I. INTRODUCTION

It is recently proposed that by simply square-rooting an existing topological phase, a completely new material displaying exotic edge states properties is obtained [1]. Inspired by Dirac's idea [2] in treating the Klein-Gordon equation [3, 4], such a square-rooting procedure is obtained by enlarging the degrees of freedom of the original system and devising a new Hamiltonian, the square of which yields two copies of the original system's Hamiltonian [1]. In the last few years, various proposals of square-root topological phases have been theoretically made [5–14] and experimentally verified [15–17]. These studies however concern only the physics of static systems.

Since the last decade, various phases of matter that can only be found in periodically driven (Floquet) systems have been identified and gained significant attention [18–33]. Apart from being of fundamental interest, novel Floquet phases have been demonstrated to yield advantages in quantum information processing [34–40]. It is thus envisioned that the possibility of square-rooting these Floquet systems will lead to even more exotic phases of matter with a significant quantum technological impact. To the best of our knowledge, however, such square-root Floquet phases have not been explored up to this date.

A static (Floquet) system is characterized by a Hermitian Hamiltonian  $H$  (unitary one-period evolution operator  $U$ ). This fundamental difference renders any known technique in square-rooting static systems inapplicable for use in Floquet setting. At first glance, square-rooting a Floquet system might even appear trivial. Indeed, by writing  $U = e^{-iH_{\text{eff}}T}$  for some effective Hamiltonian  $H_{\text{eff}}$ , its square-root is obtained simply through  $H_{\text{eff}} \rightarrow \frac{H_{\text{eff}}}{2}$ . However, it is important to note that  $H_{\text{eff}}$  is generically not physically accessible, especially for Floquet phases that have no static counterpart [24–33]. In this case,

simply reducing all system parameters by a half is not equivalent to  $H_{\text{eff}} \rightarrow \frac{H_{\text{eff}}}{2}$  and will thus not yield the desired square-rooted system.

In this paper, we propose a general procedure for square-rooting a Floquet system in a systematic way, allowing its repetition to further generate any  $2^n$ -th-root version of the system. Remarkably, unlike existing square-rooting procedures that typically only work for specific single-particle static topological systems, our proposal is applicable both to noninteracting and interacting Floquet systems, as demonstrated in the two explicit systems studied below. These case studies further reveal that such a square-rooting procedure is especially fruitful to yield systems with exotic properties that are otherwise absent in their original counterparts. For these reasons, our proposal opens an exciting opportunity to discover and study a variety of new Floquet phases.

## II. GENERAL CONSTRUCTION

The method introduced below is applicable to *any* periodically driven system whose one-period evolution (Floquet) operator can be written as

$$U = U_1 U_2 = e^{-i\frac{H_1 T}{2}} e^{-i\frac{H_2 T}{2}}, \quad (1)$$

where  $T$  is the system's period,  $H_1$  and  $H_2$  are *physically realizable* Hamiltonians. Our square-rooting procedure consists of the following two steps. First, we introduce an additional spin-1/2 degree of freedom, characterized by Pauli matrices  $\tau_j$  with  $j = x, y, z$ . Second, we define a two-time step Hamiltonian

$$h_{(1/2)}(t) = \begin{cases} M\tau_y & \text{for } n < \frac{t}{T} \leq n + \frac{1}{2} \\ H_1 \frac{1+\tau_z}{2} + H_2 \frac{1-\tau_z}{2} & \text{for } n + \frac{1}{2} < \frac{t}{T} \leq n + 1 \end{cases}, \quad (2)$$

where  $n \in \mathbb{Z}$ . Such a square-root Hamiltonian and its original counterpart are schematically shown in Fig. 1.

\* Raditya.Bomantara@sydney.edu.au

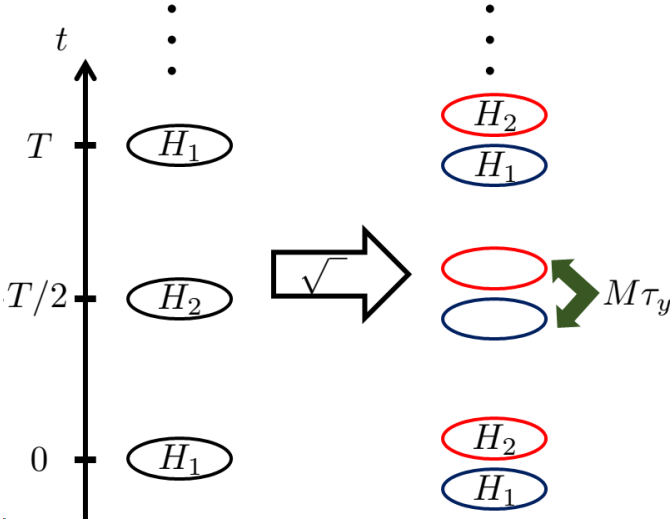


FIG. 1. Constructing a square-root Floquet system from a two-time-step parent Hamiltonian.

At  $MT = \pi$ , it is easy to verify that the Floquet operator associated with Eq. (2) takes the form

$$u_{(1/2)} = \begin{pmatrix} \mathbf{0} & e^{-i\frac{H_1 T}{2}} \\ -e^{-i\frac{H_2 T}{2}} & \mathbf{0} \end{pmatrix}. \quad (3)$$

In particular,  $u_{(1/2)}$  squares to  $\text{diag}(-U_1 U_2, -U_2 U_1)$ , thereby reproducing two decoupled copies of the target  $U$  (up to a unitary transformation). As  $MT \neq \pi$ , the diagonal elements of  $u_{(1/2)}$  may in general become nonzero, and  $u_{(1/2)}^2$  now represents two coupled copies of  $U$ . However, since our square-rooting procedure is to be applied to Floquet phases that are known to display robustness against small perturbations, it is expected that  $u_{(1/2)}^2$  still inherits the main physics of the target system. Therefore, provided that the deviation from  $MT = \pi$  is not too large, Eq. (2) can still be regarded as the square-root of the target model. In the numerics presented below, we intentionally set  $MT \neq \pi$  to support this point.

Importantly, since the above steps yield a time-periodic Hamiltonian whose Floquet operator can be written in the form of Eq. (1), our square-rooting procedure can be applied indefinitely to obtain the  $2^n$ th-root of the original periodically driven Hamiltonian. Given that a periodically driven system is known to exhibit unique properties with no static analogues [24–37], the systematic procedure elucidated above thus opens the possibility for obtaining a variety of even more exotic physical properties. For conciseness, we will focus on the square-root of some Floquet phases and demonstrate the emergence of features that are not found in the original systems. In Appendix C, the 4th- and 8th-root version of such phases are presented.

### III. SQUARE-ROOT FLOQUET TOPOLOGICAL SUPERCONDUCTOR WITH ARBITRARILY MANY EDGE MODES

A remarkable feature of periodically driven topological phases is their possibility to support any number of edge modes through appropriate choice of system parameters [41–47]. To demonstrate our square-rooting procedure at work, we consider the Floquet topological superconducting model introduced in Ref. [46], which is described by the Floquet operator of the form Eq. (1), where

$$H_\ell = \sum_{j=1}^N \mu_\ell c_j^\dagger c_j + \sum_{j=1}^{N-1} \left( -J_\ell c_j^\dagger c_{j+1} + \Delta_\ell c_j^\dagger c_{j+1}^\dagger + h.c. \right), \quad (4)$$

$\mu_\ell$ ,  $J_\ell$ , and  $\Delta_\ell$  are respectively the chemical potentials, hopping amplitudes, and pairing strengths,  $\ell = 1, 2$ ,  $c_j$  is the fermionic operator at site  $j$ , and  $N$  is the system size. In particular, at  $\mu_2 = -2J_2 = -2\Delta_2 = m\mu_1 = 2mJ_1 = 2m\Delta_1$  with  $m \in \mathbb{R}$ , such a system supports  $n$  pairs of Majorana zero modes and Majorana  $\pi$  modes (MZMs and MPMs) for  $n\pi < m < (n + \frac{1}{2})\pi$  [46]. Here, MZMs and MPMs are defined as topologically protected Hermitian edge-localized operators which respectively commute and anticommute with the system's Floquet operator  $U$  [34–36, 48–51].

Following our general construction, the corresponding square-root system is obtained as a two-time-step Hamiltonian  $h_{(1/2)}^{(FTSC)}(t)$  which switches between  $h_{(1/2),1}^{(FTSC)} = \sum_{j=1}^N \text{Mic}_{1,j}^\dagger c_{2,j} + h.c.$  and  $h_{(1/2),2}^{(FTSC)} = h_1 + h_2$  after every  $T/2$  time interval, where  $h_\ell$  with  $\ell = 1, 2$  take the form of Eq. (4) with  $c_j \rightarrow c_{\ell,j}$ . Physically, such a system represents a pair of  $p$ -wave superconductors with inter-chain hopping applied during the first half of the period. The Bogoliubov–de Gennes (BdG) Floquet operator  $\mathcal{U}$ , which is related to the actual Floquet operator via  $u = \frac{1}{2}\Psi^\dagger \mathcal{U} \Psi$ , can be explicitly obtained as

$$\mathcal{U} = e^{-i \sum_{j=1}^N \frac{MT}{2} \tau_y |j\rangle \langle j|} e^{-i \sum_{\ell=1,2} \sum_{j=1}^N \mu_\ell T \sigma_z \frac{1+(3-2\ell)\tau_z}{4} |j\rangle \langle j|} \times e^{i \sum_{\ell=1,2} \sum_{j=1}^{N-1} [(J_\ell \sigma_z - i\Delta_\ell \sigma_y) T \frac{1+(3-2\ell)\tau_z}{4} |j\rangle \langle j+1| + h.c.]}, \quad (5)$$

where  $\sigma_j$ 's and  $\tau_j$ 's are Pauli matrices in the particle-hole space and chain species respectively,  $|j\rangle$  denotes the  $j$ th site, and  $\Psi = \bigotimes_{j=1}^N \bigotimes_{\ell=1,2} \left( c_{j,\ell}, c_{j,\ell}^\dagger \right)^T$ .

The system's quasienergy ( $\varepsilon$ ) excitation spectrum is obtained from the eigenvalues  $e^{-i\varepsilon T}$  of  $\mathcal{U}$  and is summarized in Fig. 2(a). The associated quasienergy excitation spectrum of the original system (with  $\pi/T$  quasienergy shift) is plotted in Fig. 2(b) for reference. Note in particular that both systems share the same topological phase transition points, marked by parameter values at which gap closing exists. MZMs and MPMs are associated with quasienergy zero and  $\pi/T$  solutions respectively in Fig. 2(a), but they correspond to quasienergy  $\pi/T$  and zero solutions respectively in Fig. 2(b) due to the  $\pi/T$

quasienergy shift. Moreover, the following two features are clearly observed.

First, the presence of MPMs in the original system leads to the simultaneous presence of MZMs and MPMs in the square-root system. This feature can further be analytically proven by computing a pair topological invariants  $(\nu_0, \nu_\pi)$  and  $(\nu_0^{(1/2)}, \nu_\pi^{(1/2)})$  for the original and square-root system respectively. In particular,  $\nu_0$  ( $\nu_0^{(1/2)}$ ) and  $\nu_\pi$  ( $\nu_\pi^{(1/2)}$ ) respectively determine the number of pairs of MZMs and MPMs in the original (square-root) system. By leaving the technical detail in Appendix A, we indeed find that  $\nu_\pi = \nu_0^{(1/2)} = \nu_\pi^{(1/2)}$ , thus confirming our observation above.

Second, the presence of MZMs in the original system leads to the emergence of edge modes at  $\approx \pi/(2T)$  quasienergy. Recently, it was shown that such  $\pi/2$  modes may become parafermions [52, 53] in the presence of interaction [54]. These  $\pi/2$  modes are however not as ubiquitous as MZMs and MPMs, and their construction previously involves a rather elaborate driving scheme [54]. With our square-rooting procedure, such  $\pi/2$  modes can thus be systematically generated, and their origin can be traced back from the topology of the squared model. That is, while it is unknown if a topological invariant for characterizing these  $\pi/2$  modes can be constructed in the square-root system directly, the presence of  $\pi/2$  modes can still be inferred from the invariant  $\nu_0$  defined on the squared system.

Equation (5) inherits the chiral symmetry of the original (squared) model. Specifically, the operator  $\mathcal{C} = \sigma_x \tau_z$  maps  $\mathcal{C}\mathcal{U}'\mathcal{C}^{(-1)} = \mathcal{U}'^\dagger$ , where  $\mathcal{U}' \equiv e^{i\sum_{j=1}^N \frac{MT}{4}\tau_y|j\rangle\langle j|} \mathcal{U} e^{-i\sum_{j=1}^N \frac{MT}{4}\tau_y|j\rangle\langle j|}$  is the Floquet operator in a symmetric time-frame [55]. This chiral symmetry is responsible for protecting MZMs and MPMs in the system. Indeed, even at imperfect square-root parameter  $MT \neq \pi$ , which physically induces a coupling between two copies of the squared model, MZMs and MPMs remain pinned at 0 and  $\pi/T$  quasienergy respectively (see Fig. 2(a)). By contrast, the observed  $\pi/2$  modes slightly deviate from the expected  $\pi/(2T)$  quasienergy due to the absence of symmetry protection. It remains to be seen if the presence of interaction that promotes these  $\pi/2$  modes to  $Z_4$  parafermions in the ideal limit, such as via the mechanism elucidated in Ref. [54], may render them more robust against such imperfection effect.

#### IV. SQUARE-ROOT FLOQUET TIME CRYSTALS

Our construction is not limited to single-particle systems. Indeed, a Floquet time crystal (FTC), i.e., a phase of matter characterized by robust subharmonic observable dynamics [56–87], can be obtained in a periodically driven interacting spin chain whose one-period time evolution (Floquet) operator takes the form of Eq. (1). We

can thus construct its square-root counterpart by following the general prescription above. Focusing first on the many-body localization (MBL) protected FTC model in Ref. [57], we introduce the two-time-step Hamiltonian  $h_{(1/2)}^{(MBL)}(t)$  which switches between

$$h_{(1/2),1}^{(MBL)} = \sum_j (J_j Z_j Z_{j+1} + h_j^Z Z_j)(1 - \tau_z) + \sum_j h_j X_j(1 + \tau_z), \quad h_{(1/2),2}^{(MBL)} = M\tau_y, \quad (6)$$

at every  $\frac{T}{2}$  time interval. There,  $P_j = J_j, h_j, M$ , and  $h_j^Z$  are each randomly taken from a uniform set  $[\bar{P} - \Delta P, \bar{P} + \Delta P]$ ,  $X_j$  and  $Z_j$  are Pauli matrices associated with the  $j$ th site in the 1D lattice, and  $\tau_{x,y,z}$  are additional Pauli matrices. One interpretation of Eq. (6), albeit a rather unrealistic one in the thermodynamic limit, is that it describes a single spin  $(\tau_{x,y,z})$  interacting with a 1D Ising model. In a more physical setting, Eq. (6) can be effectively and more robustly realized with two interacting and periodically driven spin chains. As detailed in Appendix B, this is achieved by replacing  $Z_j \rightarrow Z_{j,A}$ ,  $X_j \rightarrow X_{j,A}X_{j,B}$ ,  $\tau_z \rightarrow Z_{j,A}Z_{j,B}$ , and  $\tau_y \rightarrow \sum_{j=1}^N X_{j,B}$  in Eq. (6), where  $A, B$  label the two chains. The resulting system can in turn be implemented with FTC successful trapped ions [59, 60] and superconducting circuit [66] platforms [86].

In Fig. 3, we plot the stroboscopic magnetization dynamics, i.e.,  $\langle S_z \rangle = \frac{1}{N} \sum_{j=1}^N \langle Z_j \rangle$ , and its associated power spectrum, i.e.,  $\langle \tilde{S}_z \rangle = |\frac{1}{L} \sum_{m=\ell}^L \langle S_z \rangle e^{-\frac{\ell\Omega T}{L}}|$ , under Eq. (6) and a generic initial state  $|\psi(0)\rangle = \prod_{j=1}^N e^{-i\frac{\pi}{8}Y_j}|00\dots 0\rangle$ . As expected from a typical FTC, robust subharmonic dynamics which improves with the system size is clearly observed even as the system parameters  $h_j$  and  $M$  deviate from their ideal values. More remarkably, it exhibits a  $4T$ - rather than  $2T$ -periodicity, thus highlighting its nature as the square-root of the FTC model in Ref. [57]. Repeating the square-rooting procedure then yields a means to create a  $2^n T$ -period FTC (see, e.g., Appendix C). Such an FTC is physically different from that proposed in Ref. [86], which is clear by the absence and presence of  $\Omega = \frac{\pi}{T}$  peak in Fig. 3 of the present paper and Fig. 2 of Ref. [86] respectively.

The advantage of our square-rooting procedure over the FTC construction proposed in Ref. [86] is the possibility to devise large-period FTCs without MBL. To support this argument, we will now present another  $4T$ -period FTC, obtained from square-rooting the disorder-free kicked Lipkin-Meshkov-Glick (LMG) model of Ref. [71]. This amounts to defining another two-time-step Hamiltonian  $h_{(1/2)}^{(LMG)}$  which switches between

$$h_{(1/2),1}^{(LMG)} = H_{LMG}(1 - \tau_z) + \sum_j \phi X_j(1 + \tau_z), \quad h_{(1/2),2}^{(LMG)} = M\tau_y \quad (7)$$

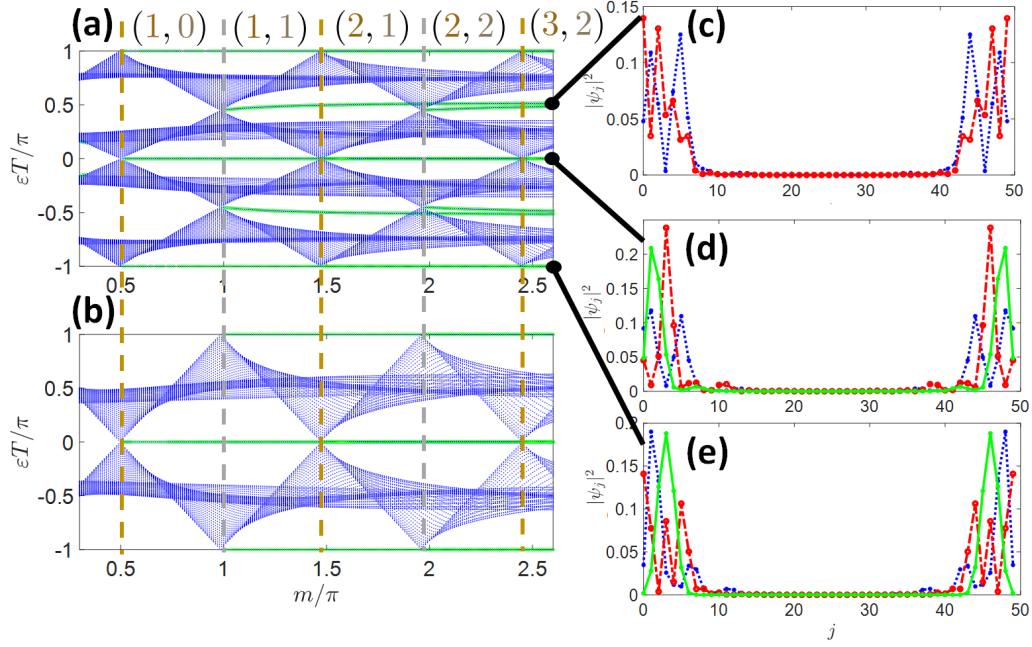


FIG. 2. Quasienergy excitation spectrum of the (a) square-root and (b) original Floquet topological superconductor of Ref. [47]. The vertical lines mark the topological phase transition points, while  $(\nu_\pi, \nu_0)$  is a pair of topological invariants determining the number of MPMs and MZMs in the original system. (c,d,e) Typical wavefunction profiles of the system's edge modes. The system parameters are chosen as  $\mu_2 T = m\mu_1 T = 2m$ ,  $-J_2 T = mJ_1 T = 1.05m$ ,  $-\Delta_2 T = m\Delta_1 T = 0.95m$ ,  $MT = 0.9\pi$ , and  $N = 50$ .

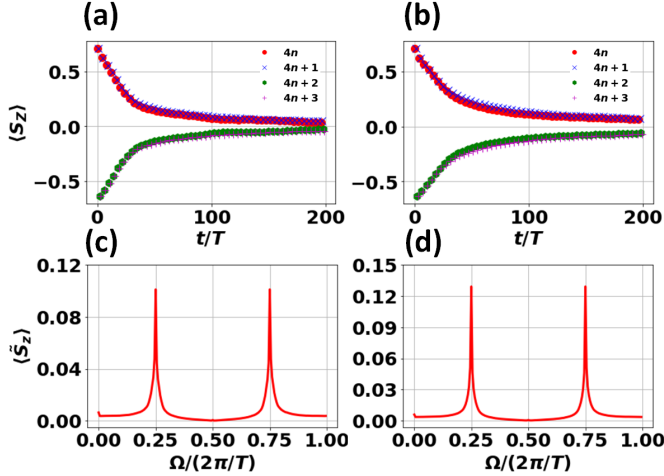


FIG. 3. Stroboscopic magnetization profile (a,b) and its associated power spectrum (c,d) under Eq. (6) after averaging over 500 disorder realizations for a system of (a,c) 8 and (b,d) 10 particles. The system parameters are chosen as  $\hbar T = \frac{0.92\pi}{2}$ ,  $\bar{J}T = 1$ ,  $\bar{h}^Z T = 0.15$ ,  $\bar{M}T = 0.95\pi$ ,  $\Delta\hbar T = \frac{0.05\pi}{2}$ ,  $\Delta JT = 0.5$ ,  $\Delta\hbar^Z T = 0.15$ , and  $\Delta MT = 0.05\pi$ .

at every  $\frac{T}{2}$  time interval, where  $H_{LMG} = \sum_{i,j} \frac{J}{2N} Z_i Z_j + \sum_i \hbar X_i$ .

Since such a system preserves the total spin  $\mathcal{S}^2 = \sum_{i,j} (X_i X_j + Y_i Y_j + Z_i Z_j)$ , numerical studies of up to

$\sim 1000$  particles are accessible via exact diagonalization. In Fig. 4, we evaluate  $\langle S_z \rangle$  stroboscopically from the initial state  $|\psi(0)\rangle = |00\cdots 0\rangle$  for various system sizes. As expected, a  $4T$  oscillation profile is clearly observed in all panels and persists longer at larger system sizes. While large period FTCs may also be found in the original kicked LMG model, they are only observable at sufficiently large system sizes [77, 78]. The square-rooted model thus allows such FTCs to be accessible at much smaller system sizes. Indeed, with a more physical and robust implementation of Eq. (7) via two interacting kicked LMG chains as detailed in Appendix B, a long-lasting  $4T$  oscillation profile is observed with merely  $\sim 10$  particles.

## V. CONCLUDING REMARKS

We have proposed a systematic construction of square root Floquet phases exhibiting exotic properties not found in the original (squared) systems. Our proposal is applicable to any (interacting or noninteracting) time-periodic system so long as its Floquet operator takes the form of Eq. (1). As a possible future work, it would be desirable to extend our square-rooting procedure to other families of time-periodic systems with a more complex Floquet operator, such as continuously driven systems [25, 77] or systems described by a multiple-time-step

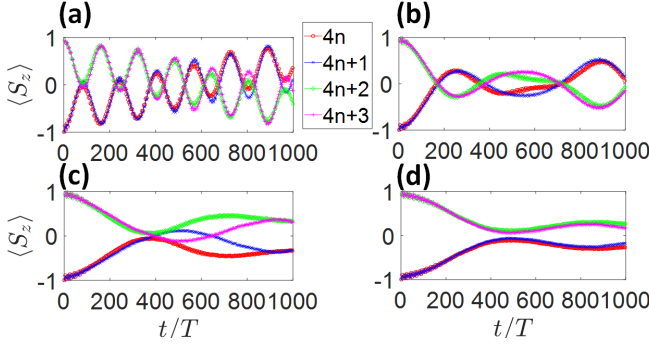


FIG. 4. Stroboscopic magnetization profile under Eq. (7) for a system of (a) 10, (b) 100, (c) 500, and (d) 1000 particles. The system parameters are chosen as  $JT = 1$ ,  $hT = 0.1$ ,  $\phi T = \frac{0.9\pi}{2}$ , and  $MT = 0.98\pi$ .

Hamiltonian [26, 33]. In a related direction, devising an alternative square-rooting procedure involving a smooth driving protocol would be beneficial for future experimental studies.

It would also be of interest to adapt the proposed procedure for  $n$ th-rooting a family of Floquet phases, where

$n \neq 2^k$  for some integer  $k$ . As an example, a cubic-root Floquet phase arising from such a procedure would be characterized by a Floquet operator that cubes to that containing three copies of the original (cubed) Floquet phase. In analogy with our proposal, we expect that this could be achieved by utilizing the  $n$ -dimensional generalizations of Pauli matrices  $\tau_y$  and  $\tau_z$  [52] in enlarging the system's degrees of freedom. In general, the ability to systematically  $n$ th-rooting Floquet systems opens the possibility for discovering various Floquet phases and understanding their physics from their parent systems. When applied to a periodically driven topological superconductor, such an  $n$ th-rooting procedure may also yield  $\pi/n$  edge modes, a main ingredient for creating Floquet parafermions [54]. The latter is particularly useful for topological quantum computing applications.

## ACKNOWLEDGMENTS

**Acknowledgement:** This work is supported by the Australian Research Council Centre of Excellence for Engineered Quantum Systems (EQUS, CE170100009).

### Appendix A: Calculation of topological invariants $\nu_0^{(1/2)}$ , and $\nu_\pi^{(1/2)}$

Under periodic boundary conditions, Eq. (5) can be written in momentum space as

$$\begin{aligned} \mathcal{U} &= \sum_k \mathcal{U}_k \otimes |k\rangle\langle k|, \\ \mathcal{U}_k &= e^{-i\frac{MT}{2}\tau_y} e^{-i\sum_{\ell=1,2}(\mu_\ell T\sigma_z \frac{1+(3-2\ell)\tau_z}{4} - (J_\ell \cos(k)\sigma_z - \Delta_\ell \sin(k)\sigma_y)T \frac{1+(3-2\ell)\tau_z}{4})}. \end{aligned} \quad (\text{A1})$$

We are particularly interested in the unitary  $\mathcal{U}'_k \equiv e^{i\frac{MT}{4}\tau_y} \mathcal{U}_k e^{-i\frac{MT}{4}\tau_y}$ , which represents the momentum space Floquet operator in the symmetric time-frame [55]. It can be rewritten as

$$\begin{aligned} \mathcal{U}'_k &= \mathcal{F}\mathcal{G}, \\ \mathcal{F} &= e^{-i\frac{MT}{4}\tau_y} e^{-i\sum_{\ell=1,2}(\mu_\ell T\sigma_z \frac{1+(3-2\ell)\tau_z}{8} - (J_\ell \cos(k)\sigma_z - \Delta_\ell \sin(k)\sigma_y)T \frac{1+(3-2\ell)\tau_z}{8})}, \\ \mathcal{G} &= \mathcal{C}\mathcal{F}^\dagger\mathcal{C}^{(-1)} = e^{-i\sum_{\ell=1,2}(\mu_\ell T\sigma_z \frac{1+(3-2\ell)\tau_z}{8} - (J_\ell \cos(k)\sigma_z - \Delta_\ell \sin(k)\sigma_y)T \frac{1+(3-2\ell)\tau_z}{8})} e^{-i\frac{MT}{4}\tau_y}, \end{aligned} \quad (\text{A2})$$

where  $\mathcal{C} = \sigma_x\tau_z$  is the chiral symmetry operator. In the following, we focus on the ideal square-root limit  $MT = \pi$ . For simplicity, we take  $\mu_2 = -2J_2 = -2\Delta_2 = m\mu_1 = 2mJ_1 = 2m\Delta_1 \equiv m\delta$  with  $m \in \mathbb{R}$ . In the canonical basis which diagonalizes  $\mathcal{C}$ , we may write

$$\mathcal{F} = \begin{pmatrix} A & B \\ C & D \end{pmatrix}, \quad (\text{A3})$$

where  $A$  and  $C$  are  $2 \times 2$  matrices whose exact expression are not very relevant to our discussion, whereas

$$\begin{aligned} B &= \frac{1}{2} \begin{pmatrix} c_+ - is_- & c_- + is_+ \\ c_- - is_+ & c_+ + is_- \end{pmatrix}, \\ D &= \frac{1}{2} \begin{pmatrix} c_+ + is_- & c_- + is_+ \\ c_- - is_+ & c_+ - is_- \end{pmatrix}, \\ c_\pm &= \cos\left(\frac{m\delta T}{4}\sqrt{2(1+\cos k)}\right) \pm \cos\left(\frac{\delta T}{4}\sqrt{2(1-\cos k)}\right), \\ s_\pm &= \sin\left(\frac{\delta T}{4}\sqrt{2(1-\cos k)}\right) \frac{1 - e^{-ik}}{\sqrt{2(1-\cos(k))}} \pm \sin\left(\frac{m\delta T}{4}\sqrt{2(1+\cos k)}\right) \frac{1 + e^{ik}}{\sqrt{2(1+\cos(k))}}. \end{aligned} \quad (\text{A4})$$

By defining  $z = \frac{\delta T}{4} \left( \sqrt{2(1 - \cos k)} - i m \sqrt{2(1 + \cos k)} \right)$ , it follows that the topological invariants  $\nu_0^{(1/2)}$  and  $\nu_\pi^{(1/2)}$  can be evaluated as [35]

$$\begin{aligned} \nu_0^{(1/2)} &= \frac{1}{2\pi i} \int_{-\pi}^{\pi} dk \text{Tr} \left( B^{-1} \frac{dB}{dk} \right), \\ &= \frac{1}{2\pi i} \int_{-\pi}^{\pi} dk \frac{1}{\cos(\text{Re}(z)) \cos(\text{Im}(z)) + i \sin(\text{Re}(z)) \sin(\text{Im}(z))} \frac{d [\cos(\text{Re}(z)) \cos(\text{Im}(z)) + i \sin(\text{Re}(z)) \sin(\text{Im}(z))]}{dk}, \\ \nu_\pi^{(1/2)} &= \frac{1}{2\pi i} \int_{-\pi}^{\pi} dk \text{Tr} \left( D^{-1} \frac{DD}{dk} \right), \\ &= \frac{1}{2\pi i} \int_{-\pi}^{\pi} dk \frac{1}{\cos(\text{Re}(z)) \cos(\text{Im}(z)) + i \sin(\text{Re}(z)) \sin(\text{Im}(z))} \frac{d [\cos(\text{Re}(z)) \cos(\text{Im}(z)) + i \sin(\text{Re}(z)) \sin(\text{Im}(z))]}{dk}. \end{aligned} \quad (\text{A5})$$

That is,  $\nu_0^{(1/2)} = \nu_\pi^{(1/2)}$ . To make further progress, we note that

$$d [\cos(\text{Re}(z)) \cos(\text{Im}(z)) + i \sin(\text{Re}(z)) \sin(\text{Im}(z))] = -\sin(\text{Re}(z)) \cos(\text{Im}(z)) dz^* + i \cos(\text{Re}(z)) \sin(\text{Im}(z)) dz. \quad (\text{A6})$$

By further turning the momentum integration into a complex contour integration, i.e.,  $\int_{-\pi}^{\pi} \rightarrow \frac{1}{2} \oint$  [46], we obtain

$$\nu_0^{(1/2)} = \nu_\pi^{(1/2)} = -\frac{1}{4\pi i} \oint \frac{\sin(\text{Re}(z)) \cos(\text{Im}(z)) dz^* - i \cos(\text{Re}(z)) \sin(\text{Im}(z)) dz}{\cos(\text{Re}(z)) \cos(\text{Im}(z)) + i \sin(\text{Re}(z)) \sin(\text{Im}(z))}. \quad (\text{A7})$$

Note that this is exactly the same expression as  $\nu_\pi$  of the original (squared) model, i.e., Eq. (A2) in Ref. [46]. This proves that the number of MPMs in the original model translates to the same number of MZMs and MPMs in the square-rooted model.

## Appendix B: Physical and robust implementation of square-root FTCs

The proposed square-rooting procedure amounts to introducing an additional spin particle interacting with the whole  $N$  particles in a 1D lattice, which may appear unrealistic in the thermodynamic limit due to the nonlocality of the interaction between two spins that are very far apart. In the following, we will show that in both MBL-protected and disorder-free FTCs considered in the main text, the resulting  $N + 1$  particles systems can instead be realized from two spin chains, each of size  $N$ , coupled only via two-body nearest-neighbor interactions. The main idea of this mapping is through the identification of  $N - 1$  stabilizer (mutually commuting) operators that can be fixed to a specific value, thus bringing the  $2^{2N}$ -dimensional Hilbert space of the two interacting spin chains down to a dimension of  $2^{N+1}$ . By identifying a set of logical operators (effective Pauli matrices) acting within this  $2^{N+1}$  subspace, Eqs. (6) and (7) in the main text can be implemented in a more physical and robust way, as further demonstrated below.

To be more specific, consider two spin chains of size- $N$  characterized by a set of Pauli matrices  $X_{j,S}$  and  $Z_{j,S}$  where  $j = 1, \dots, N$  and  $S = A, B$  label the lattice site and species respectively. Define the mutually commuting stabilizer operators  $\mathcal{S}_k = Z_{k,A} Z_{k,B} Z_{k+1,A} Z_{k+1,B}$  for  $k = 1, \dots, N - 1$ . It follows that the operators  $\bar{X}_j = X_{j,A} X_{j,B}$  and  $\bar{Z}_j = Z_{j,A}$ , where  $j = 1, \dots, N$ , as well as  $\bar{Y}_{N+1} = \prod_{j=1}^N X_{j,B}$  and  $\bar{Z}_{N+1} = Z_{1,A} Z_{1,B}$  commute with all  $\mathcal{S}_k$ . Moreover, these operators fulfill the Pauli algebra  $\{\bar{X}_j, \bar{Z}_j\} = 0$  and  $[\bar{X}_j, \bar{Z}_{j'}] = [\bar{Z}_j, \bar{Z}_{j'}] = [\bar{X}_j, \bar{X}_{j'}] = 0$  for  $j \neq j'$ , thus spanning a  $2^{N+1}$ -dimensional Hilbert space.

Equations (6) and (7) in the main text may now be realized with a system of two spin chains by identifying  $X_j \rightarrow \bar{X}_j$ ,  $Z_j \rightarrow \bar{Z}_j$ ,  $\tau_z \rightarrow \bar{Z}_{N+1}$ , and  $\tau_y \rightarrow \bar{Y}_{N+1}$ , thus resulting in the Floquet operators

$$\begin{aligned} u_{(1/2)}^{(MBL)} &= \exp \left( -i \frac{MT}{2} \prod_{j=1}^N X_{j,B} \right) \exp \left( -i \sum_j \left[ \left( \frac{J_j T}{2} Z_{j,A} Z_{j+1,A} + \frac{h_j^Z T}{2} Z_{j,A} \right) (1 - Z_{1,A} Z_{1,B}) \right. \right. \\ &\quad \left. \left. + \frac{h_j T}{2} X_{j,A} X_{j,B} (1 + Z_{1,A} Z_{1,B}) \right] \right), \\ u_{(1/2)}^{(LMG)} &= \exp \left( -i \frac{MT}{2} \prod_{j=1}^N X_{j,B} \right) \exp \left( -i \sum_j \left[ \left( \sum_i \frac{JT}{4N} Z_{i,A} Z_{j,A} + \frac{hT}{2} X_{j,A} X_{j,B} \right) (1 - Z_{1,A} Z_{1,B}) \right. \right. \\ &\quad \left. \left. + \frac{\phi T}{2} X_{j,A} X_{j,B} (1 + Z_{1,A} Z_{1,B}) \right] \right). \end{aligned} \quad (\text{B1})$$

While  $u_{(1/2)}^{(MBL)}$  and  $u_{(1/2)}^{(LMG)}$  are  $2^{2N}$ -dimensional, they commute with  $\mathcal{S}_k$  and can thus be written as a block diagonal matrix, where each block is of dimension  $2^{N+1}$ . That is,  $u_{(1/2)}^{(MBL)}$  and  $u_{(1/2)}^{(LMG)}$  actually encode multiple copies of Eqs. (6) and (7) in the main text, a fact that can be exploited to further simplify the systems and make them more robust in the following.

First, we note that the perfect square-root limit corresponds to setting  $MT = \pi$  in Eq. (B1), so that  $\exp\left(-i\frac{MT}{2}\prod_{j=1}^N X_{j,B}\right) = -i\prod_{j=1}^N X_{j,B}$ . Note that the latter can be equivalently written as  $\exp\left(-i\frac{MT}{2}\sum_{j=1}^N X_{j,B}\right)$ , which is not only more realistic due to it consisting of terms involving only a single Pauli matrix rather than an  $N$ -body Pauli interaction, but it is also more robust against imperfection in  $M$  [86]. Second, since  $\mathcal{S}_k$  are good quantum numbers, we may introduce them anywhere in Eq. (B1) whenever appropriate to simplify it. In particular, this allows us to modify  $Z_{1,A}Z_{1,B} \rightarrow \prod_{k=1}^{j-1} \mathcal{S}_k Z_{1,A}Z_{1,B} = Z_{j,A}Z_{j,B}$  in the second exponential of Eq. (B1). Together, these yield the improved Floquet operators

$$\begin{aligned} u_{(1/2)}^{(MBL)} &= \exp\left(-i\frac{MT}{2}\sum_{j=1}^N X_{j,B}\right) \exp\left(-i\sum_j \left[\left(\frac{J_{j,\text{intra}}T}{2}Z_{j,A}Z_{j+1,A} + \frac{J_{j,\text{inter}}T}{2}Z_{j,B}Z_{j+1,A} + \sum_{S=A,B} \frac{h_{j,S}^Z T}{2}Z_{j,S}\right) \right. \right. \\ &\quad \left. \left. + \frac{h_{X,j}T}{2}X_{j,A}X_{j,B} + \frac{h_{Y,j}T}{2}Y_{j,A}Y_{j,B}\right]\right), \\ u_{(1/2)}^{(LMG)} &= \exp\left(-i\frac{MT}{2}\sum_{j=1}^N X_{j,B}\right) \exp\left(-i\sum_j \left[\sum_i \frac{JT}{4N}(Z_{i,A}Z_{j,A} + Z_{i,A}Z_{j,B}) + \frac{(h+\phi)T}{2}X_{j,A}X_{j,B} + \frac{(\phi-h)T}{2}Y_{j,A}Y_{j,B}\right]\right), \end{aligned} \quad (\text{B2})$$

where we have further split the system parameters  $J_j$ ,  $h_j^Z$ , and  $h_j$  in  $u_{(1/2)}^{(MBL)}$  into  $J_{j,\text{intra}}$ ,  $J_{j,\text{inter}}$ ,  $h_{j,A}^Z$ ,  $h_{j,B}^Z$ ,  $h_{X,j}$ , and  $h_{Y,j}$  to allow imperfection from  $(1+\tau_z)$  and  $(1-\tau_z)$  in Eq. (6) of the main text. It is noted that all terms appearing in Eq. (B2) can be readily implemented in trapped ions [59, 60] or superconducting circuit [66] setups (see Ref. [86] for the explicit detail in realizing the two-body interactions in these experimental platforms). Moreover, as demonstrated in Ref. [86], the nonlocal interactions such as those appearing in  $u_{(1/2)}^{(LMG)}$  can be decomposed into nearest-neighbor interactions at the expense of prolonging the duration of a single period.

Our results are summarized in Figs. 5 and 6 for the magnetization dynamics under  $u_{(1/2)}^{(MBL)}$  and  $u_{(1/2)}^{(LMG)}$  respectively. To demonstrate the better robustness of the two interacting chains model as compared with the direct square-root model of Eq. (6) in the main text, the magnetization profile for both models at the same parameter values is presented in Fig. 5. For a comprehensive comparison, two different system sizes are considered for the case of Eq. (6) in the main text. Specifically, the system size of Fig. 5(b) is chosen as it leads to the same Hilbert space dimension as that of  $u_{(1/2)}^{(MBL)}$  in panel (a) when restricted to a stabilizer subspace of fixed  $\mathcal{S}_k$ . On the other hand, the system size of Fig. 6(c) is chosen so that the resulting spin chain contains the same number of particles, i.e., 8, as that of  $u_{(1/2)}^{(MBL)}$  in panel (a). Notably, while Fig. 5(c) demonstrates a stronger  $4T$  oscillation over Fig. 5(b) due to its larger system size, Fig. 5(a) outperforms both Figs. 5(b) and (c).

Since  $u_{(1/2)}^{(LMG)}$  no longer conserves the total spin number, very large system sizes are no longer accessible via exact diagonalization. Interestingly, however, even by considering only up to 14 particles and the same parameter values, Fig. 6 reveals a stronger  $4T$  magnetization dynamics over Fig. 4(d) in the main text which involves 1000 particles. This in turn demonstrates the potential of our square-rooting procedure to observe disorder-free large period FTCs at small system sizes, as claimed in the main text.

### Appendix C: 4th- and 8th-root models

To highlight the scalability of the square-rooting procedure described in the main text, we will now explicitly repeat the procedure two more times with respect to the square-rooted models obtained in the main text to yield the 4th- and 8th-root version of their parent Floquet phases. In the following, we will focus on the square-root Floquet topological



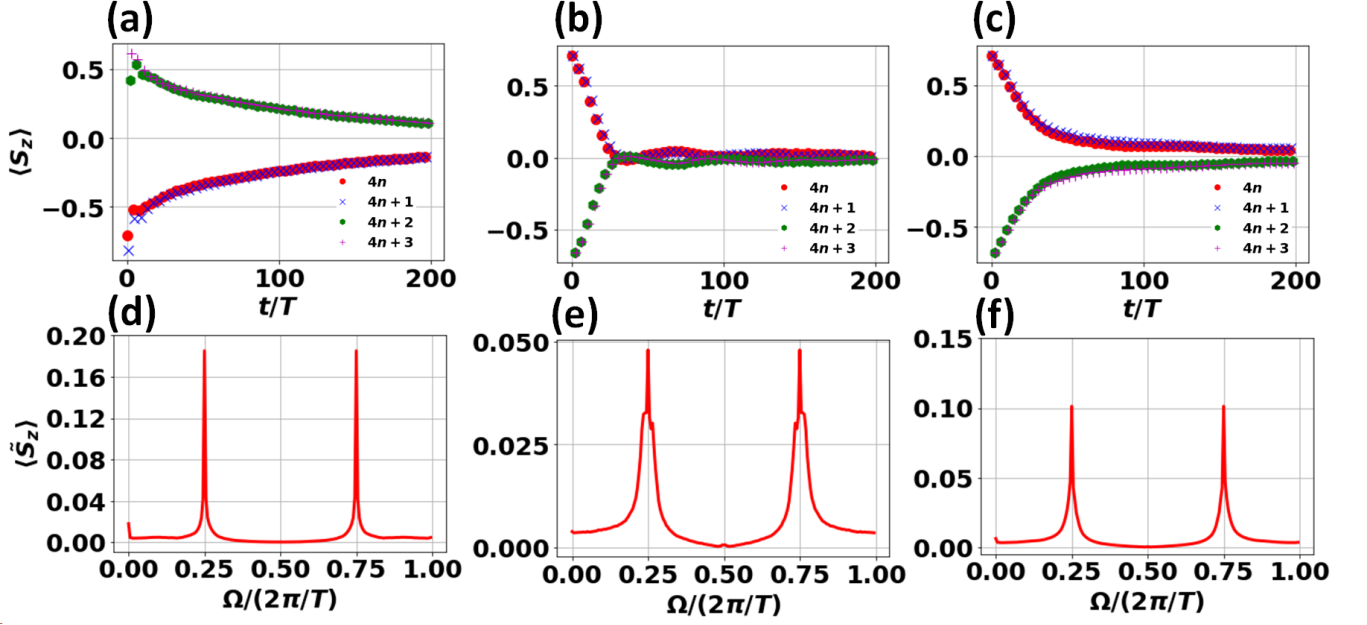


FIG. 5. (a) Stroboscopic magnetization profile under  $u_{(1/2)}^{(MBL)}$  for a system of two interacting size-4 spin chains. (b,c) Stroboscopic magnetization profile under Eq. (6) in the main text for a spin chain of size (b) 4 and (c) 8 particles. Panels (d,e,f) show the corresponding power spectrum. Each data point is averaged over 500 disorder realizations. The system parameters are chosen as  $\hbar_X T = \hbar_Y T = \frac{0.95\pi}{2}$ ,  $\bar{J}_{\text{intra}} T = \bar{J}_{\text{inter}} T = 1$ ,  $\hbar_A^Z T = \hbar_B^Z T = 0.15$ ,  $\bar{M} T = 0.95\pi$ ,  $\Delta \hbar_X T = \Delta \hbar_Y T = \frac{0.05\pi}{2}$ ,  $\Delta J_{\text{intra}} T = \Delta J_{\text{inter}} T = 0.5$ ,  $\Delta \hbar_A^Z T = \Delta \hbar_B^Z T = 0.15$ , and  $\Delta M T = 0.05\pi$ .

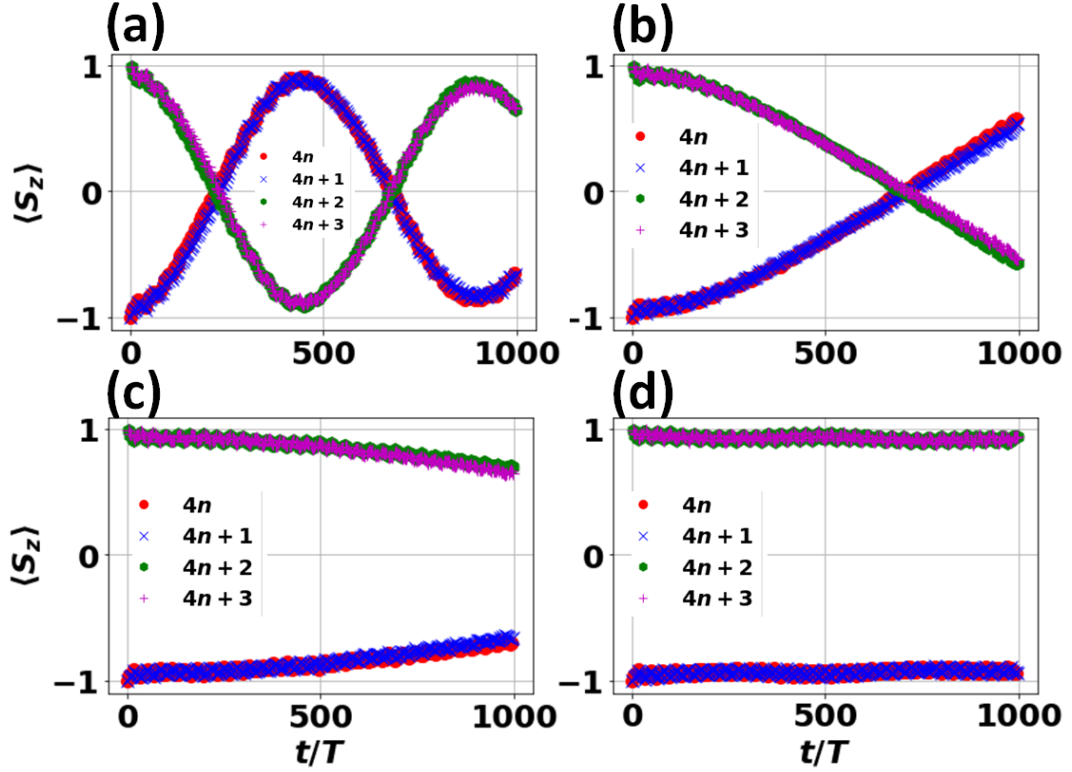


FIG. 6. Stroboscopic magnetization profile under  $u_{(1/2)}^{(LMG)}$  for a system of (a) 8, (b) 10, (c) 12, and (d) 14 particles. The system parameters are chosen as  $JT = 1$ ,  $hT = 0.1$ ,  $\phi T = \frac{0.9\pi}{2}$ , and  $MT = 0.98\pi$ .



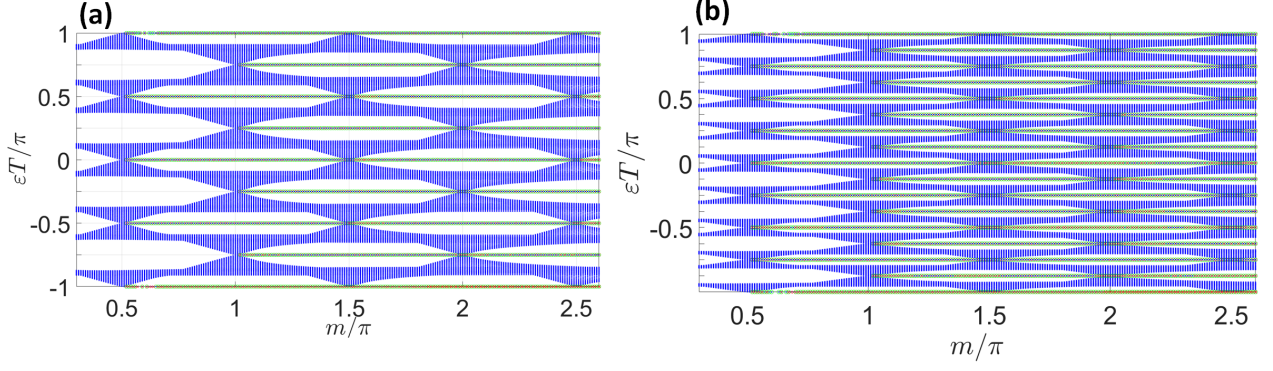


FIG. 7. Quasienergy excitation spectrum associated with (a) Eq. (C1) and (b) Eq. (C2). The system parameters are chosen as  $\mu_2 T = -2J_2 T = -2\Delta_2 T = 2m\mu_1 T = 2mJ_1 T = 2m\Delta_1 T = 2m$ ,  $MT = M'T = M''T = \pi$ , and  $N = 50$ .

superconductor of Eq. (5) in the main text and the square-root kicked LMG time crystal of Eq. (7) in the main text as a representative example of noninteracting and interacting system.

We start by devising a square-root version of Eq. (5) by introducing a new set of Pauli matrices  $\tau'_s$  ( $s = x, y, z$ ) and defining a two-time-step BdG Hamiltonian  $\mathcal{H}_{(1/4)}(t)$  which switches between

$$\begin{aligned} \mathcal{H}_{(1/4),1} = & \sum_{\ell=1,2} \sum_j \left( \mu_\ell \sigma_z \frac{1 + (3-2\ell)\tau_z}{2} |j\rangle\langle j| - \left[ (J_\ell \sigma_z - i\Delta \sigma_y) \frac{1 + (3-2\ell)\tau_z}{2} |j\rangle\langle j+1| + h.c. \right] \right) \frac{1 + \tau'_z}{2} \\ & + \sum_j M \tau_y \frac{1 - \tau'_z}{2}, \quad \mathcal{H}_{(1/4),2} = \sum_j M' \tau'_y \end{aligned} \quad (C1)$$

after every  $T/2$  time interval. We may repeat the square-rooting procedure again to obtain the time-periodic Hamiltonian  $\mathcal{H}_{(1/8)}(t)$  which switches between

$$\mathcal{H}_{(1/8),1} = \mathcal{H}_{(1/4),1} \frac{1 + \tau''_z}{2} + \mathcal{H}_{(1/4),2} \frac{1 - \tau''_z}{2}, \quad \mathcal{H}_{(1/8),2} = \sum_j M'' \tau''_y \quad (C2)$$

after every  $T/2$  time interval, where  $\tau''_s$  ( $s = x, y, z$ ) is another set of Pauli matrices. In Fig. 7, the quasienergy excitation spectrum of the two models reveals that the 4th- and 8th-root Floquet topological superconductors support  $\pi/4$  and  $\pi/8$  modes respectively. Moreover, in both models, the topological phase transitions occur at the same parameter values as the parent model of Ref. [46]. These confirm our expectation that repeated applications of our square-rooting procedure indeed yield Floquet systems with various exotic properties, i.e.,  $\pi/n$  modes, the topological origin of which can be understood from the original model.

We now turn our attention to the 4th- and 8th-root version of the kicked LMG model of Ref. [71]. To this end, we first apply our square-rooting procedure to Eq. (7) in the main text to yield a 4th-root kicked LMG time crystal described by a two-time-step Hamiltonian  $h_{(1/4)}^{(LMG)}(t)$  which switches between

$$h_{(1/4,1)}^{(LMG)} = h_{(1/2,1)}^{(LMG)} \frac{1 + \tau'_z}{2} + h_{(1/2,2)}^{(LMG)} \frac{1 - \tau'_z}{2}, \quad h_{(1/4,2)}^{(LMG)} = M' \tau'_y \quad (C3)$$

at every  $\frac{T}{2}$  time interval. Applying our square-rooting procedure one more time yields an 8th-root kicked LMG time crystal described by a two-time-step Hamiltonian  $h_{(1/8)}^{(LMG)}(t)$  which switches between

$$h_{(1/8,1)}^{(LMG)} = h_{(1/4,1)}^{(LMG)} \frac{1 + \tau''_z}{2} + h_{(1/4,2)}^{(LMG)} \frac{1 - \tau''_z}{2}, \quad h_{(1/8,2)}^{(LMG)} = M'' \tau''_y \quad (C4)$$

at every  $\frac{T}{2}$  time interval. As demonstrated in Fig. 8, robust  $8T$ - and  $16T$ -magnetization dynamics is observed for the 4th- and 8th-root kicked model respectively, thus revealing their time crystal signature. It is expected that such large-period oscillation can also be observed at much smaller system sizes by modifying  $h_{(1/4)}^{(LMG)}(t)$  and  $h_{(1/8)}^{(LMG)}(t)$  into multiple chains of interacting spin-1/2 particles following a similar procedure as that described in Sec. B.

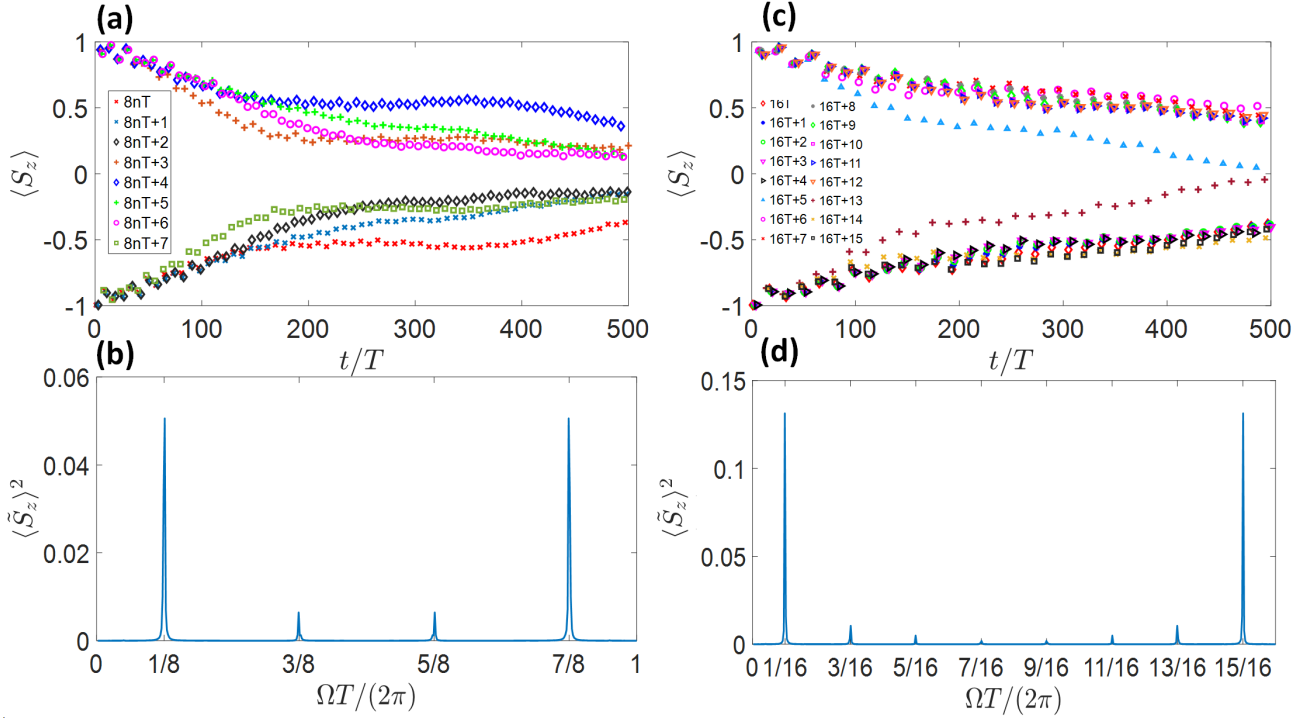


FIG. 8. (a,c) Stroboscopic magnetization profile of 200 spin-1/2 particles under (a) 4th- and (c) 8th-root kicked LMG Hamiltonian. (b,d) The associated power spectrum. The system parameters are chosen as  $JT = 1$ ,  $\hbar T = 0.1$ ,  $\phi T = \frac{0.9\pi}{2}$ ,  $MT = M'T = M''T = 0.98\pi$ .

- 
- [1] J. Arkinstall, M. H. Teimourpour, L. Feng, R. E.-Ganainy, and H. Schomerus, Phys. Rev. B **95**, 165109 (2017).
  - [2] P. A. M. Dirac, Proc. R. Soc. London A **117**, 610 (1928).
  - [3] O. Klein, Z. f Physik **41**, 407-422 (1927).
  - [4] W. Gordon, Z. f Physik **40**, 117-133 (1926).
  - [5] M. Ezawa, Phys. Rev. Res. **2**, 033397 (2020).
  - [6] T. Mizoguchi, Y. Kuno, and Y. Hatsugai, Phys. Rev. A **102**, 033527 (2020).
  - [7] A. M. Marques, L. Madail, and R. G. Dias, Phys. Rev. B **103**, 235425 (2021).
  - [8] G. Pelegrí, A. M. Marques, R. G. Dias, A. J. Daley, V. Ahufinger, and J. Mompart, Phys. Rev. A **99**, 023612 (2019).
  - [9] Z. Lin, S. Ke, X. Zhu, and X. Li, Opt. Express **29**, 8462 (2021).
  - [10] S. Ke, D. Zhao, J. Fu, Q. Liao, B. Wang, and P. Lu, IEEE J. Sel. Top. Quantum Electron **26**, 1 (2020).
  - [11] A. M. Marques and R. G. Dias, Phys. Rev. B **104**, 165410 (2021).
  - [12] T. Yoshida, T. Mizoguchi, Y. Kuno, and Y. Hatsugai, Phys. Rev. B **103**, 235130 (2021).
  - [13] T. Mizoguchi, T. Yoshida, and Y. Hatsugai, Phys. Rev. B **103**, 045136 (2021).
  - [14] R. G. Dias and A. M. Marques, Phys. Rev. B **103**, 245112 (2021).
  - [15] M. Kremer, I. Petrides, E. Meyer, M. Heinrich, O. Zilberberg, and A. Szameit, Nat. Commun. **11**, 907 (2020).
  - [16] L. Song, H. Yang, Y. Cao, and P. Yan, Nano Lett. **20**, 7566 (2020).
  - [17] M. Yan, X. Huang, L. Luo, J. Lu, W. Deng, and Z. Liu, Phys. Rev. B **102**, 180102(R) (2020).
  - [18] N. H. Lindner, G. Refael and V. Galitski, Nat. Phys. **7**, 490 (2011).
  - [19] D. Y. H. Ho and J. Gong, Phys. Rev. Lett. **109**, 010601 (2012).
  - [20] G. Jotzu, M. Messer, R. Desbuquois, M. Lebrat, T. Uehlinger, D. Greif, and T. Esslinger, Nature (London) **515**, 237 (2014).
  - [21] T. Kitagawa, M. A. Broome, A. Fedrizzi, M. S. Rudner, E. Berg, I. Kassal, A. Aspuru-Guzik, E. Demler, and A. G. White, Nat. Commun. **3**, 882 (2012).
  - [22] M. C. Rechtsman, J. M. Zeuner, Y. Plotnik, Y. Lumer, D. Podolsky, F. Dreisow, S. Nolte, M. Segev, and A. Szameit, Nature (London) **496**, 196 (2013)

- [23] J. W. McIver, B. Schulte, F.-U. Stein, T. Matsuyama, G. Jotzu, G. Meier and A. Cavalleri, Nat. Phys. **16**, 38 (2020).
- [24] D. Y. H. Ho and J. Gong, Phys. Rev. B **90**, 195419 (2014).
- [25] L. Zhou, H. Wang, D. Y. H. Ho, and J. Gong, Eur. Phys. J. B **87**, 204 (2014).
- [26] M. S. Rudner, N. H. Lindner, E. Berg, and M. Levin, Phys. Rev. X **3**, 031005 (2013).
- [27] F. Nathan and M. Rudner, New J. Phys. **17**, 125014 (2015).
- [28] R. W. Bomantara, G. N. Raghava, L. Zhou, and J. Gong, Phys. Rev. E **93**, 022209 (2016).
- [29] R. W. Bomantara and J. Gong, Phys. Rev. B **94**, 235447 (2016).
- [30] Q. Cheng, Y. Pan, H.-Q. Wang, C. Zhang, D. Yu, A. Gover, H. Zhang, T. Li, L. Zhou, and S. Zhu, Phys. Rev. Lett. **122**, 173901 (2019).
- [31] W. Zhu, H. Xue, J. Gong, Y. Chong, and B. Zhang, arXiv:2012.08847.
- [32] R. W. Bomantara, Phys. Rev. Res. **2**, 033495 (2020).
- [33] H. C. Po, L. Fidkowski, T. Morimoto, A. C. Potter, and A. Vishwanath, Phys. Rev. X **6**, 041070 (2016).
- [34] R. W. Bomantara and J. Gong, Phys. Rev. Lett. **120**, 230405 (2018).
- [35] R. W. Bomantara and J. Gong, Phys. Rev. B **98**, 165421 (2018).
- [36] R. W. Bomantara and J. Gong, Phys. Rev. B **101**, 085401 (2020).
- [37] S. Tan, R. W. Bomantara, and J. Gong, Phys. Rev. A **102**, 022608 (2020).
- [38] Z. Huang, P. S. Mundada, A. Gyeenis, D. I. Schuster, A. A. Houck, and J. Koch, Phys. Rev. Applied **15**, 034065 (2021).
- [39] P. S. Mundada, A. Gyeenis, Z. Huang, J. Koch, and A. A. Houck, Phys. Rev. Applied **14**, 054033 (2020).
- [40] Y.-S. Wang, B.-J. Liu, S.-L. Su, and M.-H. Yung, Phys. Rev. Res. **3**, 033010 (2021).
- [41] Q.-J. Tong, J.-H. An, J. B. Gong, H.-G. Luo, and C. H. Oh, Phys. Rev. B **87**, 201109(R) (2013).
- [42] L. Zhou and J. Gong, Phys. Rev. A **97**, 063603 (2018).
- [43] L. Zhou and J. Gong, Phys. Rev. B **98**, 205417 (2018).
- [44] L. Zhou and J. Gong, Phys. Rev. B **97**, 245430 (2018).
- [45] L. Zhou, Phys. Rev. B **101**, 014306 (2020).
- [46] R. W. Bomantara and J. Gong, J. Phys. Condens. Matter **32**, 435301 (2020).
- [47] R. W. Bomantara, L. Zhou, J. Pan, and J. Gong, Phys. Rev. B **99**, 045441 (2019).
- [48] L. Jiang, T. Kitagawa, J. Alicea, A. R. Akhmerov, D. Pekker, G. Refael, J. I. Cirac, E. Demler, M. D. Lukin, and P. Zoller, Phys. Rev. Lett. **106**, 220402 (2011).
- [49] D. E. Liu, A. Levchenko, and H. U. Baranger, Phys. Rev. Lett. **111**, 047002 (2013).
- [50] H.-Q. Wang, M. N. Chen, R. W. Bomantara, J. Gong, and D. Y. Xing, Phys. Rev. B **95**, 075136 (2017).
- [51] Z. Yang, Q. Yang, J. Hu, and D. E. Liu, Phys. Rev. Lett. **126**, 086801 (2021).
- [52] P. Fendley, J. Stat. Mech. **11**, P11020 (2012).
- [53] J. Alicea and P. Fendley, Annu. Rev. Condens. Matter Phys. **7**, 119 (2016).
- [54] R. W. Bomantara, Phys. Rev. B **104**, L121410 (2021).
- [55] J. K. Asbóth, B. Tarasinski, P. Delplace, Phys. Rev. B **90**, 125143 (2014).
- [56] K. Sacha, Phys. Rev. A **91**, 033617 (2015).
- [57] D. V. Else, B. Bauer, and C. Nayak, Phys. Rev. Lett. **117**, 090402 (2016).
- [58] D. V. Else, B. Bauer, and C. Nayak, Phys. Rev. X **7**, 011026 (2017).
- [59] J. Zhang, P. W. Hess, A. Kyprianidis, P. Becker, A. Lee, J. Smith, G. Pagano, I.-D. Potirniche, A. C. Potter, A. Vishwanath, N. Y. Yao, and C. Monroe, Nature (London) **543**, 217 (2017).
- [60] A. Kyprianidis, F. Machado, W. Morong, P. Becker, K. S. Collins, D. V. Else, L. Feng, P. W. Hess, C. Nayak, G. Pagano, N. Y. Yao, and C. Monroe, Science **372**, 1192-1196 (2021).
- [61] S. Choi, J. Choi, R. Landig, G. Kucsko, H. Zhou, J. Isoya, F. Jelezko, S. Onoda, H. Sumiya, V. Khemani, C. v. Keyserlingk, N. Y. Yao, E. Demler, and M. D. Lukin, Nature (London) **543**, 221 (2017).
- [62] J. Rovny, R. L. Blum, and S. E. Barrett, Phys. Rev. Lett. **120**, 180603 (2018).
- [63] J. Rovny, R. L. Blum, and S. E. Barrett, Phys. Rev. B **97**, 184301 (2018).
- [64] S. Pal, N. Nishad, T. S. Mahesh, and G. J. Sreejith, Phys. Rev. Lett. **120**, 180602 (2018).
- [65] S. Autti, P. J. Heikkinen, J. T. Mäkinen, G. E. Volovik, V. V. Zavjalov and V. B. Eltsov, Nat. Mater. **20**, 171 (2020).
- [66] Google Quantum AI and collaborators, arXiv:2107.13571v1.
- [67] V. Khemani, A. Lazarides, R. Moessner, and S. L. Sondhi, Phys. Rev. Lett. **116**, 250401 (2016).
- [68] N. Y. Yao, A. C. Potter, I.-D. Potirniche, and A. Vishwanath, Phys. Rev. Lett. **118**, 030401 (2017).
- [69] W. W. Ho, S. Choi, M. D. Lukin, and D. A. Abanin, Phys. Rev. Lett. **119**, 010602 (2017).
- [70] B. Huang, Y.-H. Wu, and W. V. Liu, Phys. Rev. Lett. **120**, 110603 (2018).
- [71] A. Russomanno, F. Iemini, M. Dalmonte, and R. Fazio, Phys. Rev. B **95**, 214307 (2017).
- [72] F. Machado, D. V. Else, G. D. K.-Meyer, C. Nayak, N. Y. Yao, Phys. Rev. X **10**, 011043 (2020).
- [73] K. Giergiel, A. Kosior, P. Hannaford, K. Sacha, Phys. Rev. A **98**, 013613 (2018).
- [74] K. Giergiel, T. Tran, A. Zaheer, A. Singh, A. Sidorov, K. Sacha, P. Hannaford, New J. Phys. **22**, 085004 (2020).
- [75] A. Russomanno, S. Notarnicola, F. M. Surace, R. Fazio, M. Dalmonte, M. Heyl, Phys. Rev. Res. **2**, 012003 (2020).
- [76] F. Iemini, A. Russomanno, J. Keeling, M. Schiro, M. Dalmonte, R. Fazio, Phys. Rev. Lett. **121**, 035301 (2018).
- [77] P. Nurwanto, R. W. Bomantara, and J. Gong, Phys. Rev. B **100**, 214311 (2019).
- [78] A. Pizzi, J. Knolle, and A. Nunnenkamp, Nat. Commun. **12**, 2341 (2021).
- [79] A. Kuros, R. Mukherjee, W. Golletz, F. Sauvage, K. Giergiel, F. Mintert, K. Sacha, New J. Phys. **22**, 095001 (2020).
- [80] J. Wang, P. Hannaford, and B. J. Dalton, New J. Phys. **23**, 063012 (2021).
- [81] K. Sacha, *Time Crystals* (Springer, Switzerland, 2020).

- [82] D. V. Else, C. Monroe, C. Nayak, and N. Y. Yao, *Annu. Rev. Condens. Matter Phys.* **11**, 467-499 (2020).
- [83] V. Khemani, R. Moessner, S. L. Sondhi, [arXiv:1910.10745v1](https://arxiv.org/abs/1910.10745v1).
- [84] K. Sacha, J. Zakrzewski, *Rep. Prog. Phys.* **81**, 016401 (2017).
- [85] L. Guo and P. Liang, *New. J. Phys.* **22**, 075003 (2020).
- [86] R. W. Bomantara, *Phys. Rev. B* **104**, L180304 (2021).
- [87] R. W. Bomantara, *Phys. Rev. B* **104**, 064302 (2021).